8. J. M. Caruge, J. E. Halpert, V. Wood, V. Bulovic, M. G. Bawendi, *Nat. Photonics* **2**, 247 (2008).
9. E. H. Sargent, *Nat. Photonics* **3**, 325 (2009).
10. X. B. Chen, Y. Lou, A. C. Samia, C. Burda, *Nano Lett.* **3**, 799 (2003).
11. X. G. Peng, M. C. Schlamp, A. V. Kadavanich, A. P. Alivisatos, *J. Am. Chem. Soc.* **119**, 7019 (1997).
12. Z. L. Wang, *J. Phys. Chem. B* **104**, 1153 (2000).
13. C. J. Palmstrøm, *Annu. Rev. Mater. Sci.* **25**, 389 (1995).
14. J. S. Lee, E. V. Shevchenko, D. V. Talapin, *J. Am. Chem. Soc.* **130**, 9673 (2008).
15. H. Kim, M. Achermann, L. P. Balet, J. A. Hollingsworth, V. I. Klimov, *J. Am. Chem. Soc.* **127**, 544 (2005).
16. T. Mokari, C. G. Sztrum, A. Salant, E. Rabani, U. Banin, *Nat. Mater.* **4**, 855 (2005).
17. T. Mokari, E. Rothenberg, I. Popov, R. Costi, U. Banin, *Science* **304**, 1787 (2004).
18. C. Wang, C. Xu, H. Zeng, S. Sun, *Adv. Mater.* **21**, 3045 (2009).
19. Materials and methods are available as supporting material on *Science* Online.
20. A. M. Smith, A. M. Mohs, S. Nie, *Nat. Nanotechnol.* **4**, 56 (2009).
21. J. Zhang, Y. Tang, L. Weng, M. Ouyang, *Nano Lett.* **9**, 4061 (2009).
22. R. G. Pearson, *J. Am. Chem. Soc.* **85**, 3533 (1963).
23. M. Misono, E. Ochiai, Y. Saito, Y. Yoneda, *J. Inorg. Nucl. Chem.* **29**, 2685 (1967).
24. C. E. Anson *et al.*, *Angew. Chem. Int. Ed.* **47**, 1326 (2008).
25. D. H. Son, S. M. Hughes, Y. Yin, A. Paul Alivisatos, *Science* **306**, 1009 (2004).
26. U. Y. Jeong, Y. N. Xia, Y. D. Yin, *Chem. Phys. Lett.* **416**, 246 (2005).
27. J. D. Hoffman, *J. Chem. Phys.* **29**, 1192 (1958).
28. D. Turnbull, *J. Appl. Phys.* **21**, 1022 (1950).
29. J. K. Bording, J. Tafto, *Phys. Rev. B* **62**, 8098 (2000).
30. A. L. Pan *et al.*, *J. Phys. Chem. B* **110**, 22313 (2006).
31. K. T. Shimizu, W. K. Woo, B. R. Fisher, H. J. Eisler, M. G. Bawendi, *Phys. Rev. Lett.* **89**, 117401 (2002).
32. Y. D. Jin, X. H. Gao, *Nat. Nanotechnol.* **4**, 571 (2009).
33. P. P. Pompa *et al.*, *Nat. Nanotechnol.* **1**, 126 (2006).

34. This work was supported by Office of Naval Research YIP award (N000140710787), NSF CAREER award (DMR-0547194), and Beckman YIP grant (0609259093). Facility support was from Maryland Nanocenter and its Nanoscale Imaging Spectroscopy and Properties Laboratory (supported in part by the NSF as a Materials Research Science and Engineering Center shared experiment facility). We also thank G. Jenkins, T. Einstein, and J. R. Anderson for reading and polishing the manuscript.

Supporting Online Material

www.sciencemag.org/cgi/content/full/327/5973/1634/DC1
Materials and Methods
SOM Text
Figs. S1 to S13
Tables S1 and S2
References

16 November 2009; accepted 11 February 2010
10.1126/science.1184769

Shaping Development of Autophagy Inhibitors with the Structure of the Lipid Kinase Vps34

Simon Miller,[1] Brandon Tavshanjian,[2] Arkadiusz Oleksy,[1] Olga Perisic,[1] Benjamin T. Houseman,[2] Kevan M. Shokat,[2] Roger L. Williams[1]*

Phosphoinositide 3-kinases (PI3Ks) are lipid kinases with diverse roles in health and disease. The primordial PI3K, Vps34, is present in all eukaryotes and has essential roles in autophagy, membrane trafficking, and cell signaling. We solved the crystal structure of Vps34 at 2.9 angstrom resolution, which revealed a constricted adenine-binding pocket, suggesting the reason that specific inhibitors of this class of PI3K have proven elusive. Both the phosphoinositide-binding loop and the carboxyl-terminal helix of Vps34 mediate catalysis on membranes and suppress futile adenosine triphosphatase cycles. Vps34 appears to alternate between a closed cytosolic form and an open form on the membrane. Structures of Vps34 complexes with a series of inhibitors reveal the reason that an autophagy inhibitor preferentially inhibits Vps34 and underpin the development of new potent and specific Vps34 inhibitors.

The class III phosphoinositide 3-kinase (PI3K), Vps34, is the most ancient paralog of the three classes of PI3Ks in mammals (*1*). It engages in a wide range of intracellular transport activities, including transport to lysosomes via multivesicular bodies (*2*), endosome–to–trans-Golgi transport via retromers (*3*), phagosome maturation (*4*, *5*), and autophagy (*6*). More recently, signaling roles of Vps34 have been described in nutrient sensing in the mammalian target of rapamycin (mTOR) pathway (*7*, *8*) and signaling downstream of heterotrimeric GTP-binding protein–coupled receptors (*9*). Given the role of Vps34 in activating mTOR signaling, Vps34 inhibitors could have application in treatment of obesity or insulin resistance (*10*). One of the obstacles to understanding the cellular roles of Vps34 is that, currently, there is no inhibitor capable of specifically inhibiting class III PI3K.

Vps34 phosphorylates the D-3 hydroxyl of the phospholipid phosphatidylinositol (PtdIns) to produce PtdIns3P. Proteins containing binding domains such as FYVE or PX that specifically recognize PtdIns3P initiate the assembly of complexes at the membranes of endosomes, phagosomes, or autophagosomes. Vps34 associates with the N-terminally myristoylated, putative Ser/Thr protein kinase Vps15 (hVps15/p150 in humans), which leads to activation of Vps34 (*11*, *12*). Regulatory proteins such as Rab5 and Rab7 bind to Vps15 and enable activation of the Vps34/Vps15 complex at membranes (*6*, *13*, *14*).

The Vps34/Vps15 heterodimer is found in multiple complexes in eukaryotes (*10*), some of which have a fundamental role in autophagy (*15*). Autophagy has diverse intracellular roles, including degradation of long-lived proteins and organelles and also in maintaining a balance between cell growth and death during development (*16*, *17*). In yeast, Vps15/Vps34/Vps30 form the core of complexes I and II, whereas the autophagy proteins Atg14 and Vps38 recruit this core for autophagy and endosome-to-TGN (trans-Golgi network) sorting, respectively (*18*). The mammalian ortholog of Vps30 is Beclin1, which in autophagy associates with hAtg14/Barkor (*19*, *20*) and, in a separate complex, ultraviolet irradiation resistance–associated gene (UVRAG) (*21*) and Bax-interacting factor-1 (Bif-1) (*22*). UVRAG has also been proposed to function in endosomal sorting (*23*).

A construct of *Drosophila melanogaster* Vps34 (DmVps34) lacking the C2 domain (Δ1-257), referred to as HELCAT (helical and catalytic domains), was used for the 2.9 Å resolution structure determination (Fig. 1A) (*24*). The C2 domain had no influence on catalytic activity in vitro (figs. S1 and S2), but its role may be to bind Beclin1 (*21*). The overall fold of the enzyme showed a solenoid helical domain packed against a catalytic domain, forming a compact unit with extensive interdomain contacts (Fig. 1B). The asymmetric unit of the crystals contains a dimer of Vps34 with 1800 Å^2 of the solvent-accessible surface buried in the interface. The C-terminal helix of one subunit inserts into a prominent slot on the surface of the other subunit (fig. S3). However, light-scattering analyses indicate that Vps34 is a monomer in solution (fig. S4).

One of the most notable features of the Vps34 structure is the completely ordered phosphoinositide-binding or "activation" loop (Fig. 1, B to E, and fig. S5). This loop is critical for the characteristic lipid substrate preferences of the PI3K catalytic subunits (*25*), but in other PI3K structures, it has been largely disordered (*26*, *27*). The proximal (N-terminal) end of the Vps34 activation loop forms an essential part of the phosphotransferase reaction center (Fig. 1, C to E). The intermediate section forms a vertical wall reaching toward the membrane surface (Fig. 1E). The distal (C-terminal) end of the loop cradles the C-terminal helix from the other molecule in the crystal dimer. Although we have been unable to obtain a Vps34/PtdIns complex structure, it is possible to model phosphoinositide headgroup binding that would facil-

[1]Medical Research Council Laboratory of Molecular Biology, Hills Road, Cambridge CB2 0QH, UK. [2]Howard Hughes Medical Institute and Department of Cellular and Molecular Pharmacology, University of California San Francisco (UCSF), 600 16th Street, MC2280, San Francisco, CA 94158, USA.

*To whom correspondence should be addressed. E-mail: rlw@mrc-lmb.cam.ac.uk

itate direct transfer of the adenosine triphosphate (ATP) γ-phosphate to the 3-OH of the inositol ring (Fig. 1C). The 1-phosphate of the substrate is likely to be adjacent to the ε-amino group of Lys^{771}-Hs (Lys^{833}-Dm) at the apex of the loop, which is consistent with our observation that the $Lys^{771} \rightarrow Ala^{771}$ (K771A) mutant dramatically impairs activity (Fig. 2A). The inositol ring would stack on the hydrophobic surface created by Pro^{770}-Hs and Tyr^{764}-Hs (832-Dm and 826-Dm) (Fig. 1C). Consistent with this finding, the $Tyr^{764} \rightarrow Ala^{764}$ mutation inactivates the enzyme (Fig. 2A). The D-3 hydroxyl would be in a small pocket lined with catalytic loop residues Asp^{743}-Hs, Arg^{744}-Hs, His^{745}-Hs, and Asn^{748}-Hs (Dm 805-DRHxxN-810). The guanidinium group of Arg^{744}-Hs interacts with, and potentially stabilizes, the backbone of the Asp-Phe-Gly (DFG) motif in the activation loop, and the positive charge may also help neutralize negative charge in the transition state of γ-phosphate transfer.

Vps34 residues within the conserved catalytic loop DRH motif (Hs 743-DRH-745 and Dm 805-807) have a conformation that suggests a mechanism whereby His^{745}-Hs could act as the catalytic base, abstracting a proton from the substrate 3-OH to facilitate nucleophilic attack on the γ-phosphate of ATP. Two acidic residues, Asp^{743}-Hs and Asp^{761}-Hs (Asp^{805}-Dm and Asp^{823}-Dm) are well positioned to act as metal ligands that could help neutralize negative charge in the transition state (Fig. 2B). The p110γ/ATP structure appears to have captured the catalytic loop in an inactive state in which neither the histidine nor the aspartate of the DRH is properly oriented for catalysis. The difference between the p110γ and Vps34 catalytic loops may reflect an inactive-to-active transition that is possible for all PI3Ks (Fig. 2C).

An earlier study noted the importance of a C-terminal element for Vps34 activity in vivo (*28*). The structure shows that this element is part of the C-terminal helix (kα12). This helix has a critical role in catalysis both in vitro (Fig. 2A) and in vivo (Fig. 2D). Truncation of the 10 C-terminal residues of human and yeast Vps34 almost completely abrogates catalytic activity. Even single point mutations in the conserved C-terminal motif ΦHxΦxQxWRx greatly reduce enzymatic activity on PtdIns-containing vesicles (Fig. 2A) and in vivo (Fig. 2D). Surprisingly, truncation of the 10 C-terminal residues enhances basal ATPase activity in the absence of lipid substrate (Fig. 2E). The HsVps34 $Trp^{885} \rightarrow Ala^{885}$ and $Tyr^{884} \rightarrow Ala^{884}$ mutations in the C terminus also increase the basal ATPase activity (Fig. 2E). This suggests that, in the closed form, the C-terminal helix would fold over the catalytic loop locking the catalytic His^{745}-Hs (His^{807}-Dm) in its inactive conformation (Fig. 3A). In this arrangement, the C-terminal helix would be cradled by the activation loop (fig. S3). Consistent with this point, the activation-loop mutant K771A increases basal ATPase activity like the C-terminal helix mutations. The loop between the last two helices would act as a hinge that enables a closed-to-open form transition (Fig. 3B). Consequently, the C-terminal tail appears to have a dual role: auto-inhibitory off the membrane and activating on the membrane. Fluorescence resonance energy transfer and lipid sedimentation analyses also show that the C-terminal helix has a role in membrane binding (fig. S6).

The Vps34 ATP-binding pocket (Fig. 4A) has a smaller volume than the corresponding pocket of the class I p110γ pocket (800 versus 1200 $Å^3$). In Vps34, the P loop [known to bind the phosphates of ATP (*26*)] curls inward toward the ATP-binding pocket, and this is coincident with a parallel inward bending of the kα1/kα2

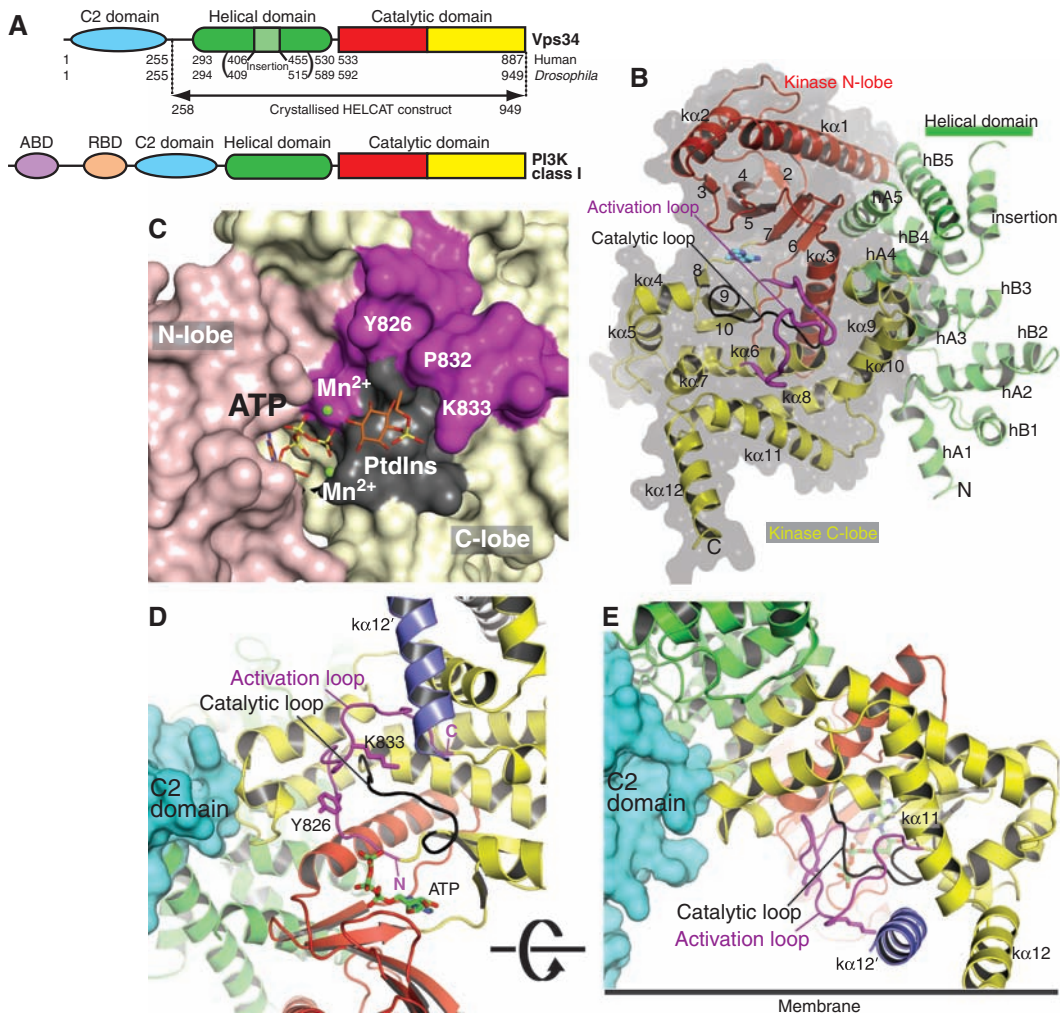

Fig. 1. Structure of Vps34 catalytic core (HELCAT). (**A**) Domain organization of Vps34 and class I PI3Ks. (**B**) Overall fold of the DmVps34 HELCAT. (**C**) Model for PtdIns headgroup binding to Vps34, suggesting that Lys^{833}-Dm (Lys^{771}-Hs) interacts with the 1-phosphate (*30*). (**D**) View of the hook-shaped activation loop (magenta) encircling the catalytic loop (black). The C2 domain (light blue) is that of p110γ after superimposing DmVps34 residues 291 to 949 onto p110γ. The kα12′ helix (gray) is the C-terminal helix from the adjacent molecule in the crystal dimer. (**E**) The putative orientation of Vps34 on a membrane.

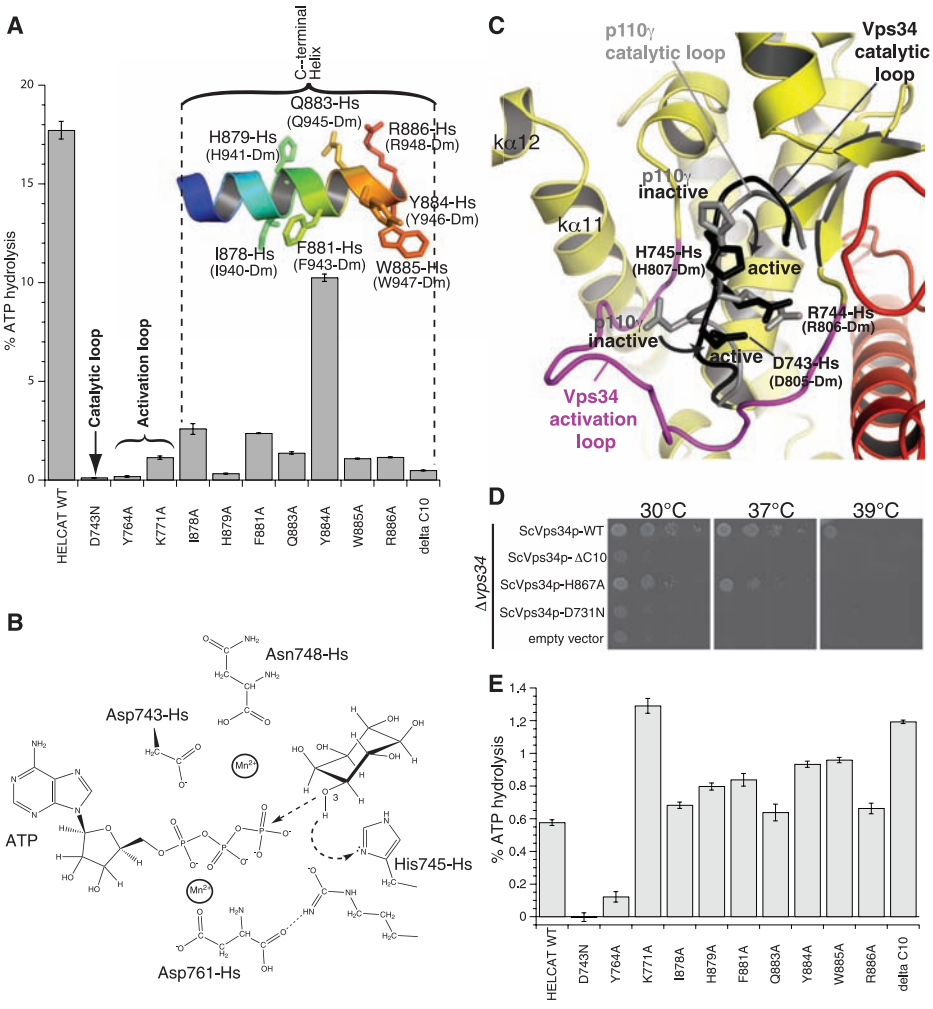

Fig. 2. Essential structural elements for Vps34 catalysis. (**A**) Catalytic activity of human wild-type HELCAT and mutant constructs on PtdIns:PS vesicles. Error bars indicate SD for triplicate assays. (**B**) Proposed catalytic mechanism of Vps34. (**C**) Close-up view of the proposed movements of catalytic loop residues His^{745}-Hs and Asp^{743}-Hs between the inactive and active conformations represented by the p110γ (gray) and DmVps34 (black) crystal structure, respectively. (**D**) The ability of a yeast Vps34p-expressing plasmid to complement the growth defect of a Δ*vps34* yeast strain at elevated temperatures is impaired by deletion of the C-terminal helix (Vps34p-ΔC10), a point mutation in this helix (ScH867A), or a mutation in the catalytic loop (ScD731N). (**E**) Basal ATPase activities in the absence of vesicles.

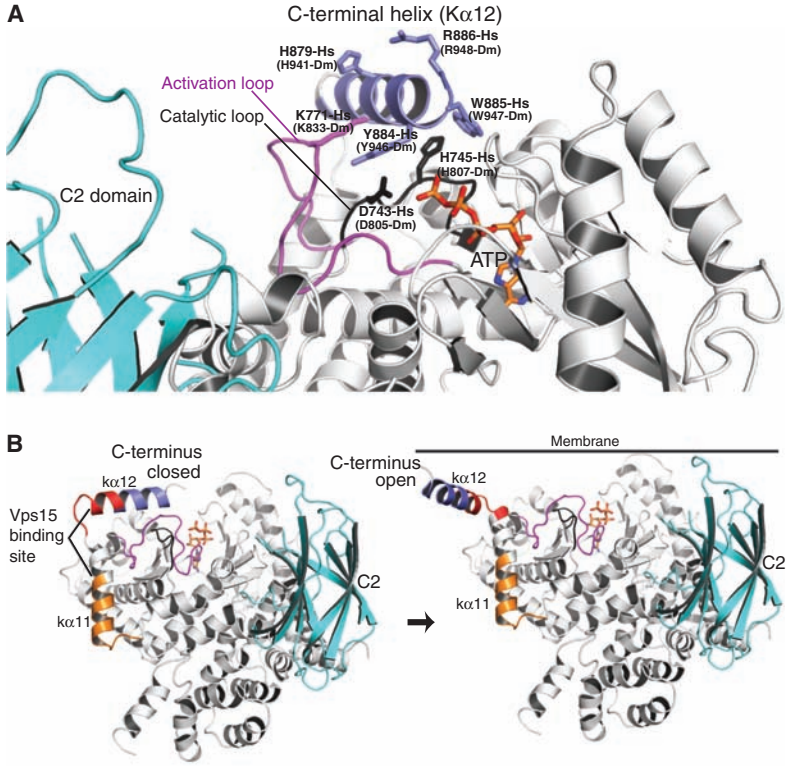

Fig. 3. A model for Vps34 activation on membranes. (**A**) Close-up view for the closed form of the enzyme in the cytosol. The C-terminal helix protects the phosphotransferase center from water. (**B**) The transition of the enzyme from a closed form in the cytosol (C-terminal helix in) to an open form with the C-terminal helix interacting with the membrane. The C2 domain (light blue) is modeled as in Fig. 1. Vps15-interacting regions are classified as strong (red) or weak (orange) (*28*).

loop (fig. S7). Furthermore, the hinge between the N and C lobes is one residue shorter in Vps34 than in class I PI3Ks; therefore, it lacks the bulged-out space at the adenine-binding pocket hinge, which is characteristic of class I PI3Ks (fig. S8).

Class I PI3Ks can form an allosteric or "specificity" pocket (adjacent to the adenine pocket) only in the presence of propeller-like inhibitors (*29*). The half-maximal inhibitory concentrations (IC_{50}s) for the propeller-like PI3K inhibitors (e.g., PIK-39) (fig. S9) are generally much worse for Vps34 than other PI3Ks. This is probably due to increased rigidity of the Vps34 pocket arising from a bulky residue substituted in the P loop (Phe^{612}-Hs, Phe^{673}-Dm) that packs against the aromatic hinge residue unique to Vps34 (Phe^{684}-Hs, Tyr^{746}-Dm). These differences effectively close off a corner of the adenine-binding pocket, giving it a more constrained appearance.

Currently there is no high-affinity, specific inhibitor of Vps34. We determined the structure of a complex of Vps34 with 3-methyladenine (3-MA) (Fig. 4, B and C), which is often used as a specific inhibitor of autophagy. We also determined the structures of Vps34 in complexes with three multi-targeted inhibitors: (i) PIK-90, (ii) PIK-93, (iii) and PI-103 (Fig. 4, D to F). These complexes provide insight into developing more potent and specific Vps34 inhibitors.

Although 3-MA inhibits both class I and III PI3Ks at the 10 mM concentration typically used for inhibiting autophagy in cells, in vitro assays show that 3-MA has a preference for Vps34 (fig. S9). There is a hydrophobic ring consisting of Phe^{673}-Dm, Tyr^{746}-Dm, and Leu^{812}-Dm that encircles the 3-methyl group of 3-MA and is unique to and conserved in Vps34. The corresponding residues in class I PI3Ks are not in close proximity of the 3-methyl group, and the methionine equivalent of Leu^{812}-Dm may cause steric hindrance (Fig. 4, B and C). 3-MA appears to bind to the hinge, as does the adenine moiety of ATP in p110γ, hydrogen bonding to the Val^{747}-Dm amide, and the Gln^{745} carbonyl.

All PI3K inhibitors have at least one canonical bond to the hinge. PIK-90 and PI-103 form a single H-bond, whereas PIK-93 forms two H-bonds to Val^{747}-Dm, coinciding with a lower IC_{50} of PIK-93 relative to PIK-90 (fig. S9). The affinity pocket of PI3Ks is lined with several hydrophobic and polar residues with which inhibitors can interact to greatly augment their potency, including Lys^{698}-Dm (modified by wortmannin), Asp^{823}-Dm (from the DFG), and Asp^{706}-Dm (in helix kα3, equivalent to helix αC of protein kinases). The pyridine ring of PIK-90, the chlorophenyl group of PIK-93, and the *m*-phenol group of PI-103 are within hydrogen-bonding distance of these residues. In addition, the pyridinylfuranopyrimidine group of PI-103 extends out of the pocket over the surface analogous to hydrophobic region II in protein kinases.

Our initial attempts to synthesize new Vps34 inhibitors, based on the structure of Vps34, indicate that there are ample opportunities to improve their chemical properties and substantially increase specificity for class III PI3Ks. Elaborating the ethanolamine moiety of the PIK-93 sulphonamide (compound 3-94B) that extends out of the affinity pocket and simultaneous elaborations of the sulphonamide and the amide (compound 3-94C) have little impact on IC_{50} values (fig. S10).

To exploit potential differences within the affinity pocket between Vps34 and class I PI3Ks, we increased the steric bulk of the chloro-substituent of the central phenyl ring of PIK-93. Addition of the methoxy group (compound PT21) showed little change in IC_{50} for Vps34 (88 nM), but more than a 10-fold increase in IC_{50} for the most potently inhibited class I PI3K (p110γ, 61 nM) compared with PIK-93 (fig. S10). To further improve specificity for Vps34, we synthesized an analog of PT21 with additional modifications oriented toward the hinge-region differences between Vps34 and PI3Kγ (fig. S8). Compound PT210 (fig. S10) contains a cyclopentanecarboxamide substitution for the acetamide moiety of PIK-93 and exhibits a modest 13-fold loss in potency for Vps34 (IC_{50} = 450 nM) compared with PIK-93, yet PT210 has an 1100-fold higher IC_{50} for PI3Kγ (IC_{50} ~ 4 μM) compared with PIK-93, resulting in a compound with reversed kinase specificity compared with PIK-93.

The structure of Vps34, with a completely ordered phosphoinositide-recognition loop, has enabled us to model substrate binding and the catalytic mechanism. The C-terminal helix plays a critical role in catalysis on membranes. In addition, it also has an auto-inhibitory role that prevents ATP hydrolysis when it is not at the membrane. The structures of Vps34 in complexes with PI3K inhibitors have provided clues as to how 3-MA can preferentially inhibit Vps34, and they have illustrated how additional moieties can be incorporated into inhibitors without affecting affinity for the enzyme, while greatly increasing their specificity for Vps34. This can be crucial in the design of new generations of Vps34 inhibitors with improved specificity, solubility, and cellular availability.

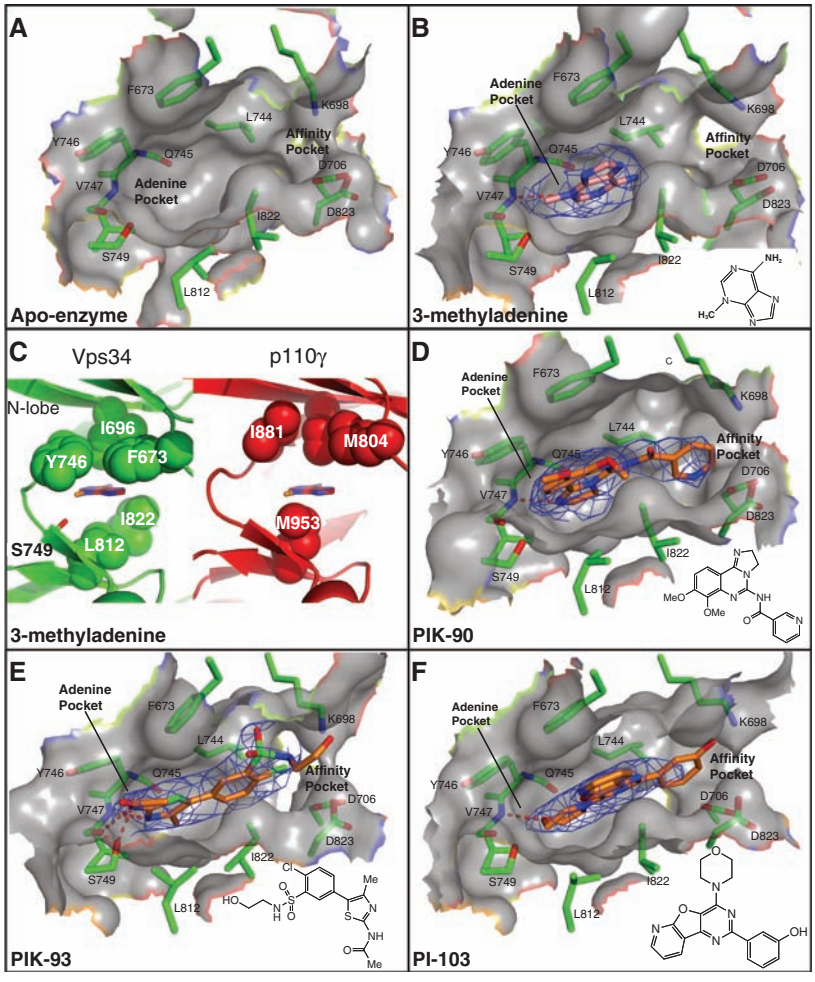

Fig. 4. Inhibitor binding in the ATP pocket. (**A**) Apo-enzyme. (**B**, **D** to **F**) Inhibitor binding with 2mFo-DFc electron densities shown (contoured at 1.0σ). (**C**) A comparison of the ATP-binding pocket of the Vps34/3-MA complex (left, green) with p110γ (right, red). A ring of hydrophobic residues encircles 3-MA and may provide specificity for Vps34. The p110γ structure shown is PDB ID 1E8X, but a 3-MA has been placed in the pocket as a reference point for comparison with the Vps34/3-MA complex.

References and Notes

1. J. A. Engelman, J. Luo, L. C. Cantley, *Nat. Rev. Genet.* **7**, 606 (2006).
2. P. V. Schu *et al.*, *Science* **260**, 88 (1993).
3. P. Burda, S. M. Padilla, S. Sarkar, S. D. Emr, *J. Cell Sci.* **115**, 3889 (2002).
4. O. V. Vieira *et al.*, *J. Cell Biol.* **155**, 19 (2001).
5. I. Vergne *et al.*, *Proc. Natl. Acad. Sci. U.S.A.* **102**, 4033 (2005).
6. A. Simonsen, S. A. Tooze, *J. Cell Biol.* **186**, 773 (2009).
7. M. P. Byfield, J. T. Murray, J. M. Backer, *J. Biol. Chem.* **280**, 33076 (2005).
8. T. Nobukuni *et al.*, *Proc. Natl. Acad. Sci. U.S.A.* **102**, 14238 (2005).
9. J. E. Slessareva, S. M. Routt, B. Temple, V. A. Bankaitis, H. G. Dohlman, *Cell* **126**, 191 (2006).
10. J. M. Backer, *Biochem. J.* **410**, 1 (2008).
11. C. Panaretou, J. Domin, S. Cockcroft, M. D. Waterfield, *J. Biol. Chem.* **272**, 2477 (1997).
12. Y. Yan, R. J. Flinn, H. Wu, R. S. Schnur, J. M. Backer, *Biochem. J.* **417**, 747 (2009).
13. H. W. Shin *et al.*, *J. Cell Biol.* **170**, 607 (2005).
14. J. T. Murray, J. M. Backer, *Methods Enzymol.* **403**, 789 (2005).
15. K. Obara, T. Sekito, Y. Ohsumi, *Mol. Biol. Cell* **17**, 1527 (2006).
16. E. L. Axe *et al.*, *J. Cell Biol.* **182**, 685 (2008).
17. G. M. Fimia *et al.*, *Nature* **447**, 1121 (2007).
18. A. Kihara, T. Noda, N. Ishihara, Y. Ohsumi, *J. Cell Biol.* **152**, 519 (2001).
19. E. Itakura, C. Kishi, K. Inoue, N. Mizushima, *Mol. Biol. Cell* **19**, 5360 (2008).
20. Q. Sun *et al.*, *Proc. Natl. Acad. Sci. U.S.A.* **105**, 19211 (2008).
21. C. Liang *et al.*, *Nat. Cell Biol.* **8**, 688 (2006).
22. Y. Takahashi *et al.*, *Nat. Cell Biol.* **9**, 1142 (2007).
23. C. Liang *et al.*, *Nat. Cell Biol.* **10**, 776 (2008).
24. Materials and methods are available as supporting material on *Science* Online.
25. T. Bondeva *et al.*, *Science* **282**, 293 (1998).
26. E. H. Walker, O. Perisic, C. Ried, L. Stephens, R. L. Williams, *Nature* **402**, 313 (1999).
27. C.-H. Huang *et al.*, *Science* **318**, 1744 (2007).
28. Y. V. Budovskaya, H. Hama, D. B. DeWald, P. K. Herman, *J. Biol. Chem.* **277**, 287 (2002).
29. A. Berndt *et al.*, *Nat. Chem. Biol.* **6**, 117 (2010).
30. Single-letter abbreviations for the amino acid residues are as follows: A, Ala; C, Cys; D, Asp; E, Glu; F, Phe; G, Gly; H, His; I, Ile; K, Lys; L, Leu; M, Met; N, Asn; P, Pro; Q, Gln; R, Arg; S, Ser; T, Thr; V, Val; W, Trp; and Y, Tyr.

31. We thank European Synchrotron Radiation Facility beamline scientists for ID14-4, ID23-1, and ID29. We are grateful to Y. Ohashi and A. Gillingham for help with yeast experiments, C. Sachse for electron microscopy, M. Allen for help with x-ray data collection, A. Berndt for advice and discussions, S. Munro for critically reading the manuscript, B. González for a clone of HsVps34, and G. Ducker for help in optimizing Vps34 inhibitor assays. B.T.H. is supported by the Mount Zion Health Fund, B.T. is supported by the Achievement Rewards for College Scientists Fellowship at UCSF, and K.M.S. thanks the Waxman Foundation for support. The coordinates have been deposited in the Protein Data Bank, with the following identification numbers (PDB IDs): 2X6H (apo), 2X6I (PIK-90), 2X6J (PIK-93), 2X6K (PI-103), and 2X6F (3-MA).

Supporting Online Material

www.sciencemag.org/cgi/content/full/327/5973/1638/DC1
Materials and Methods
Figs. S1 to S11
Table S1
References

9 November 2009; accepted 26 February 2010
10.1126/science.1184429

Evolutionary Trade-Offs in Plants Mediate the Strength of Trophic Cascades

Kailen A. Mooney,[1]* Rayko Halitschke,[2] Andre Kessler,[2] Anurag A. Agrawal[2,3]

Predators determine herbivore and plant biomass via so-called trophic cascades, and the strength of such effects is influenced by ecosystem productivity. To determine whether evolutionary trade-offs among plant traits influence patterns of trophic control, we manipulated predators and soil fertility and measured impacts of a major herbivore (the aphid *Aphis nerii*) on 16 milkweed species (*Asclepias* spp.) in a phylogenetic field experiment. Herbivore density was determined by variation in predation and trade-offs between herbivore resistance and plant growth strategy. Neither herbivore density nor predator effects on herbivores predicted the cascading effects of predators on plant biomass. Instead, cascade strength was strongly and positively associated with milkweed response to soil fertility. Accordingly, contemporary patterns of trophic control are driven by evolutionary convergent trade-offs faced by plants.

Trophic cascades—the indirect positive effect of predators on plant biomass through herbivore suppression—are the best examples of the importance of indirect interactions as determinants of community structure and ecosystem function. For this reason, there has been great interest in elucidating the sources of variation in trophic cascade strength both within (*1*–*3*) and among ecosystems (*4*). Much of the research aimed at explaining variation in trophic cascade strength has focused on factors mediating the top-down effects of predators on herbivores, including the influences of intraguild predation (*5*), synergistic and antagonistic effects of multiple predators (*6*), trophic subsidies to predators (*7*), and the nonconsumptive effects of predators on herbivores (*8*). At the same time, it is also recognized that plant stoichiometry (*9*), antiherbivore defense traits (*10*–*12*), and primary productivity (*13*, *14*) can mediate trophic cascade strength from the bottom up. Consequently, a consensus is emerging that multiple, complementary top-down and bottom-up processes determine trophic cascade strength.

Although it is recognized that plant traits can influence interactions with herbivores and herbivore-predator interactions (*15*, *16*), there has been little consideration of how plant growth and defense strategies might result in predictable patterns of trophic cascade strength. There is wide acceptance that plant species evolve in response to fundamental trade-offs that should influence the effects of predators and productivity upon herbivore and plant biomass. For example, plant defense theory predicts that fast-growing species should have relatively low herbivore resistance as compared with slow-growing species (*17*, *18*). Plant resistance to herbivores may in turn influence the indirect effects of predators on plants by altering herbivore susceptibility to predators (*19*, *20*). Similarly, plant growth strategies influence tolerance to herbivory (*21*, *22*), again showing potential to alter the strength of trophic cascades. Although trophic cascades are rightly considered community-level phenomena (*23*), an understanding of how plant traits influence such dynamics requires first documenting the influence of plant traits on component, species-level cascades.

We conducted a field experiment in which we grew 16 species of milkweeds (*Asclepias* spp., Apocynaceae) (Fig. 1), factorially manipulated predator access and soil fertility, and monitored plant biomass and populations of the potent herbivore *Aphis nerii* (Aphididae, Hemiptera), a specialist on the Apocynaceae that occurs naturally on the studied milkweeds (*24*). It has previously been shown that milkweed species influence this aphids' population dynamics and interactions with parasitoids (*16*, *25*). We tested whether there are indirect consequences of such variation in trophic dynamics for plant growth as well as whether trade-offs between milkweed growth strategy and herbivore resistance predictably influence the top-down effects of predators. Because all plants were grown in a single environment, any variation in the effects of predators and growth strategy can be attributed to plant species traits. By interpreting these patterns of interspecific variation in trophic structure from a phylogenetic perspective, we link the outcome of fundamental evolutionary trade-offs to contemporary community dynamics.

We first tested for variation among milkweed species in the effects of predators and soil fertility on both plant biomass and herbivore abundance using general linear models. Where species varied in such responses, we then quantified effect sizes for individual species [log response ratios (*26*)] in order to examine the relationships among species using phylogenetically independent contrasts (*27*).

[1]Department of Ecology and Evolutionary Biology, University of California, Irvine, CA 92697–2525 USA. [2]Department of Ecology and Evolutionary Biology, Cornell University, Ithaca, NY 14853–2701 USA. [3]Cornell Center for a Sustainable Future, Ithaca, NY 14853, USA.

*To whom correspondence should be addressed. E-mail: mooneyk@uci.edu

Shaping Development of Autophagy Inhibitors with the Structure of the Lipid Kinase Vps34

Simon Miller, Brandon Tavshanjian, Arkadiusz Oleksy, Olga Perisic, Benjamin T. Houseman, Kevan M. Shokat and Roger L. Williams

Science **327** (5973), 1638-1642.
DOI: 10.1126/science.1184429

Lipid Kinase Revealed

The lipid kinase, Vps34, makes the key signaling lipid phosphatidylinositol 3-phosphate [PI(3)P] and has essential roles in autophagy, membrane trafficking, and cell signaling. It is a class III PI 3-kinase, a class against which there is currently no specific inhibitor. **Miller *et al.*** (p. 1638) now describe the crystal structure of Vps34. Modeling substrate binding and combining structural data with mutagenesis suggests a mechanism in which Vps34 is auto-inhibited in solution, but adopts a catalytically active conformation on membranes. Structures of Vps34 with existing inhibitors might allow for the generation of inhibitors with high affinity and specificity.